View metadata, citation and similar papers at core.ac.uk
brought to you by CORE
provided by HZB Repository

JOURNAL OF APPLIED PHYSICS **100**, 023710 (2006)

ZnO layers deposited by the ion layer gas reaction on Cu(In,Ga)(S,Se)$_2$ thin film solar cell absorbers: Morphology, growth mechanism, and composition

M. Bär,[a),b)] J. Reichardt,[a),c)] I. Sieber, A. Grimm, I. Kötschau, I. Lauermann, S. Sokoll, M. C. Lux-Steiner,[d)] and Ch.-H. Fischer[d)]
Solarenergieforschung, Hahn-Meitner-Institut Berlin, Glienicker Strasse 100, D-14109 Berlin, Germany

T. P. Niesen
Shell Solar GmbH, Otto-Hahn-Ring 6, D-81739 Munich, Germany

(Received 5 July 2005; accepted 31 May 2006; published online 24 July 2006)

Cu(In,Ga)(S,Se)$_2$ (CIGSSe) based solar cells with a ZnO window extension layer (WEL) deposited by the ion layer gas reaction (ILGAR) reach competitive efficiencies compared to corresponding references with CdS buffer and lead to a simplified device structure. The WEL replaces not only the CdS buffer, but also the undoped part of the usually applied rf-sputtered ZnO window bilayer. Since the performance of corresponding solar cell devices depends strongly on the ILGAR process parameters (number of deposition cycles and process temperature), respective ILGAR-ZnO/CIGSSe test structures were investigated by means of scanning electron microscopy and x-ray photoelectron spectroscopy. Thereby, the growth mechanism of ILGAR-ZnO on CIGSSe absorbers and its morphology was investigated. In addition, the surface composition was determined, showing that ILGAR-ZnO layers contain a certain amount of metastable hydroxide. Due to the systematic variation of the ILGAR process parameters it could be demonstrated that it is possible to directly tune the hydroxide content in the ILGAR-ZnO layers. © *2006 American Institute of Physics*. [DOI: 10.1063/1.2218032]

I. INTRODUCTION

Many attempts have been made to replace the heavy metal compound CdS in chalcopyrite-based thin film solar cells by a non toxic and more transparent material, promising higher efficiencies. Conventional CdS-containing Cu(In$_{(1-X)}$Ga$_X$)(S$_Y$Se$_{(1-Y)}$)$_2$ (CIGSSe) solar cell devices reach efficiencies up to 19.5% (Ref. 1) [for Cu(In,Ga)Se$_2$, $Y=0$] on the laboratory scale (0.41 cm^2). Those high efficiency solar cells consist of a *p*-type CIGSSe absorber (conduction type inverted near the surface[2]) and a CdS buffer layer, which is usually deposited in a chemical bath (CBD). Conventionally, the solar cell device is completed by a zinc oxide (ZnO) window bilayer consisting of a highly *n*-doped ZnO (n^+-ZnO) on top of an intrinsic, undoped ZnO layer (*i*-ZnO), both generally deposited by sputtering. One promising approach to replace the CdS buffer is the window extension layer (WEL) concept,[3] which means that not only the CBD-CdS layer, but also the intrinsic part of the window bilayer is replaced by one layer: the WEL. This concept is implemented by a ZnO WEL. In order to fulfill the requirements of a buffer layer, the WEL is not deposited by the conventionally used rf sputtering, but by the "softer" ion layer gas reaction (ILGAR) technique.[4–6] ILGAR is a material efficient, nonvacuum, sequential and cyclic, wet chemical, low cost deposition method more suitable for industrial in-line mass production than, e.g., CBD. The ILGAR deposition process starts with dipping of the substrate in a precursor salt solution (usually a metal salt solved in an organic solvent.). After evaporation of the solvent the remaining (dry) solid salt is converted by a NH$_3$/H$_2$O gas mixture into the corresponding hydroxide.[6] Thus, while the application of the precursor salt onto the substrate is executed wet chemically, the actual chemical reaction takes place at a solid/gas interface. The number of process cycles ("dips") determines the layer thickness and by the process temperature [according to Eq. (1)] the extent of dehydration and thereby the oxide/hydroxide ratio of the deposited

$$\mathrm{Zn(OH)_2} \xrightarrow{\text{energy}} \mathrm{ZnO + H_2O} \quad (1)$$

layer[7–9] is controlled. Recently, we could demonstrate[10] that exposing hydroxide-rich layers to a synchrotron beam ($h\nu = 654$ eV) also initiates their dehydration. The ILGAR WEL is rather a Zn(O,OH) compound than pure ZnO, especially for low process temperatures. Nevertheless, for simplicity we will still refer to this material as ILGAR-ZnO.

Figure 1 shows the dependence of the photovoltaic (PV) parameters (short circuit current density J_{sc}, open circuit voltage V_{oc}, fill factor FF, and power conversion efficiency η) of solar cell devices with ILGAR-ZnO WELs on the ILGAR process parameters: namely, the number of process cycles [see Fig. 1(a), data taken from Ref. 3 presenting the mean value of the best six (out of 8) cells] and the process temperature [see Fig. 1(b), data taken from Ref. 7 presenting

[a)]Authors to whom correspondence should be addressed.
[b)]Present address: Department of Chemistry, University of Nevada, Las Vegas (UNLV), 4505 Maryland Parkway, Las Vegas, NV 89154-4003; electronic mail: baerm2@unlv.nevada.edu
[c)]Present address: Complex Systems Lab, Universität Bremen, Otto-Hahn-Allee, 28359 Bremen, Germany; electronic mail: reichardt@uni-bremen.de
[d)]Also at: Freie Universität Berlin, D-14195 Berlin, Germany.

 © 2006 American Institute of Physics

Downloaded 31 Aug 2007 to 134.30.24.17. Redistribution subject to AIP license or copyright, see http://jap.aip.org/jap/copyright.jsp

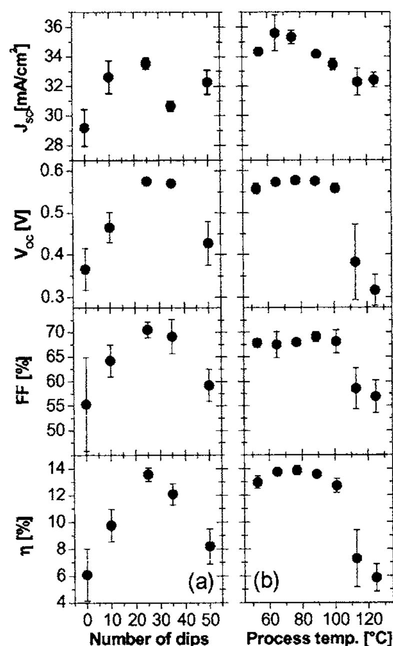

FIG. 1. Mean PV parameter (short circuit current density J_{sc} open circuit voltage V_{oc} fill factor FF, and power conversion efficiency η) of CIGSSe-based solar cells with ILGAR-ZnO WEL depending on the ILGAR process parameters: Number of process cycles (a) and process temperature (b). Data taken from Ref. 3 and 7, respectively. The process temperature for the dip variation was 100 °C and the temperature variation was done with 30 dip ILGAR-ZnO WELs. The total area (0.5 cm^2) PV parameters were determined under standard test conditions (AM 1.5, 25 °C, and 100 mW/cm^2). The error bars visualize the standard deviation from the mean value of at least six cells.

the mean value of 16 cells]. Note that the efficiency of solar cells with an ILGAR-ZnO WEL (prepared by 25 dips at 75 °C) is fairly competitive to that of respective CBD-CdS references (14.6% for the device made according to the WEL concept compared to 14.8% for the CdS buffered solar cell).[7] Thus, the WEL concept simplifies the device structure making one complete high vacuum process step obsolete without loss in device performance.

However, the PV parameters of solar cell devices with ILGAR-ZnO WELs strongly depend on the deposition parameters of the ILGAR process (see Fig. 1). In order to investigate this behavior, scanning electron microscopy (SEM) and x-ray photoelectron spectroscopy (XPS) measurements were performed on ILGAR-ZnO/Cd^{2+}+NH_3-treated CIGSSe test structures. Note, that the Cd^{2+}/NH_3 surface treatment[11] of the absorber, which takes place prior to the actual ZnO-deposition is a standard procedure for highly efficient solar cells with ILGAR-ZnO (Refs. 3, 7, and 12) and thus included in the preparation of the test structures. The experiments were focused on the impact of the process parameters (number of deposition cycles and process temperature) on the morphology and composition of the ILGAR-ZnO layers. In addition, a model for the growth mechanism of ILGAR-ZnO on Cd^{2+}/NH_3-treated CIGSSe absorbers is developed. The results of these experiments are finally correlated with the photovoltaic parameters of corresponding solar cells.

In Ref. 13, the impact of "damp-heat" (DH) conditions (85% relative humidity at 85 °C), which are used for accelerating possible aging effects in solar cell devices, on the properties of respective ILGAR-ZnO layers is described.

II. EXPERIMENT

All experiments were based on CIGSSe/Mo/glass absorber substrates from the pilot line of Shell Solar GmbH. The CIGSSe is formed by rapid thermal annealing of stacked elemental layers on Mo-coated soda-lime glass in a sulfur-containing atmosphere.[14] For the experiments, the 60×90 cm^2 absorber plates were cut into smaller samples ($1/2 \times 1$ in.). The CIGSSe substrates were Cd^{2+}/NH_3 treated[12] prior to the actual ILGAR-ZnO deposition similar to the standard WEL solar cell preparation.[3] The treatment solution consists of $CdSO_4$ (1.5 mM, Aldrich) dissolved in aqueous ammonia (1.5 M, Merck, all chemicals were of analytical grade).[11] The sample is immersed in this treatment bath for 10 min while it is heated from room temperature up to 80 °C. Afterwards the sample is rinsed in 150 ml water and dried in a nitrogen flow. The ZnO layers were deposited at 90 °C within 10–150 ILGAR process cycles ("dips") or within 20 dips at process temperatures between 40 and 185 °C, respectively, using a precursor solution of $Zn(ClO_4)_2$ (20 mM, Aldrich)+acetonitrile (Merck). (Note, that the number of ILGAR cycles is used as measure of layer thickness. The growth rate is ~1 nm/dip.[15]) Details of the optimization of the ILGAR deposition process for ZnO WELs applied in CIGSSe based devices can be found elsewhere.[3,6,7] For comparison, an (intrinsic) ZnO reference (~15 nm) was prepared by rf sputtering from an intentionally undoped ZnO target (rf*i*-ZnO).

The morphology of the ILGAR-ZnO layers was investigated by means of SEM using a HITACHI S-4100 FE-SEM with cold field emission cathode (acceleration voltage 5 kV). The surface composition of the ILGAR-ZnO layers was analyzed in a UHV chamber (base pressure: $<5 \times 10^{-9}$ mbar) by XPS using an Mg $K\alpha$ source. The emitted photoelectrons were detected with a CLAM4 electron spectrometer from Thermo VG Scientific. The electron spectrometer was calibrated according to Ref. 6 using photoemission and Auger line positions of different metals (Cu $3p$, Au $4f_{7/2}$, Cu L_3MM, and Cu $2p_{3/2}$).

III. RESULTS AND DISCUSSION

A. Variation of the number of process cycles

1. Morphology and coverage

First, the morphology of ILGAR-ZnO layers on Cd^{2+}/NH_3-treated CIGSSe substrates is investigated by means of SEM. The respective images of ILGAR-ZnO samples prepared at 90 °C within a different number of process cycles (0–150 dips) are shown in Fig. 2, indicating a "special" growth mechanism of the ILGAR layers. The growth starts with a homogeneous layer already covering the rough (Cd^{2+}/NH_3-treated) absorber surface shown in Fig. 2(a) after ten deposition cycles [Fig. 2(b)]. This "bottom" ILGAR-ZnO layer follows the rough substrate surface quite well, reproducing the absorber morphology. For samples prepared within up to 25 dips [Figs. 2(b) and 2(c)] these layers

Downloaded 31 Aug 2007 to 134.30.24.17. Redistribution subject to AIP license or copyright, see http://jap.aip.org/jap/copyright.jsp

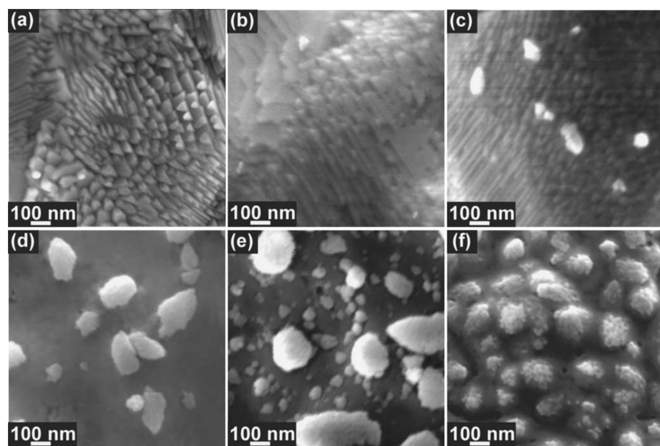

FIG. 2. SEM images of a Cd^{2+}/NH_3-treated CIGSSe absorber: uncovered and with a (a) 10 (b), 25 (c), 50 (d), 100 (e), 150 dips and (f) ILGAR-ZnO layer, all deposited at 90 °C.

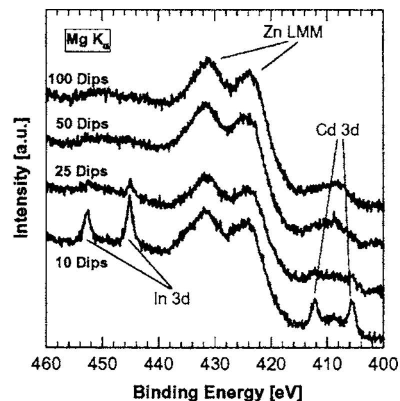

FIG. 3. XPS spectra (region of the In 3d and Cd 3d XPS lines and the Zn $L_{23}M_{23}M_{23}$ Auger line) of ILGAR-ZnO deposited at 90 °C on Cd^{2+}/NH_3-treated CIGSSe absorbers within 10, 25, 50, and 100 dips.

still mirror the faceted absorber surface underneath. For thicker layers (more than 25 dips) one can identify two different morphologies: Larger crystallites can now be observed within the so-called bottom layer increasing in size and quantity with increasing number of dips [Figs. 2(c)–2(f)]. For ILGAR-ZnO deposited within 150 dips these embedded crystallites completely dominate the layer structure [Fig. 2(f)].

In previous experiments,[17] samples prepared using 25 dips but at 100 °C process temperature were analyzed by SEM and additionally by transmission electron microscopy (TEM). Whereas the SEM images showed a similar morphology as the bottom layer in the present investigation, the TEM measurements and the determined lattice plane spacing of detected crystallites, respectively, revealed that the bottom layer consists of ZnO nanocrystallities in an amorphous matrix. Since we found a remaining hydroxide content[9] in the ILGAR-ZnO layers prepared even at this temperature (100 °C), the amorphous matrix is interpreted as $Zn(OH)_2$. In this regard, the comparatively large crystallites shown in Figs. 2(c)–2(f) are interpreted as ZnO. As a consequence, one expects a dip-dependent shift to a more oxide-rich composition with increasing layer thickness. Section III A 2 (below) gives complementary evidence for this dependency.

However, a surface modification of the CIGSSe absorbers by a simple Cd^{2+}/NH_3 treatment[18] has a distinct impact on the morphology and on the structure as well as on the composition of the deposited ILGAR-ZnO layers.[17] Furthermore it was previously shown[7–9] that the process temperature determines the extent of dehydration and thus the ratio of crystalline ZnO to amorphous $Zn(OH)_2$. Hence, it can be concluded that the deliberately altered CIGSSe surface, together with the relatively low process temperature of 90 °C, which leads to hydroxide-rich ILGAR-ZnO, are responsible for the observed special growth of the ILGAR layers. It is noted that ILGAR-ZnO deposited at 180 °C on a Si substrate grows columnarlike.[19]

As a crosscheck of the complete coverage of the CIGSSe absorber by the ILGAR layers as suggested by the SEM images in Fig. 2, the respective samples were also investigated by XPS using Mg K_α excitation. In contrast to the rather local information provided by the SEM images (Fig. 2), the corresponding XPS spectra gather surface sensitive information from almost the complete samples. In Fig. 3, spectra are exemplarily given for the 10, 25, 50, and 100 dip ILGAR-ZnO/Cd^{2+}+NH_3-treated CIGSSe samples: They show the region of the In 3d (452.6 and 445.0 eV), Cd 3d (412.1 and 405.3 eV) XPS lines, and the Zn $L_{23}M_{23}M_{23}$ (431.0 and 423.0 eV) Auger signals. (The Cd 3d signal stems from a CdS monolayer formed during the Cd^{2+}/NH_3 pretreatment on the CIGSSe surface, which has been discussed elsewhere.[18]) For the ILGAR-ZnO layer which is deposited within ten process cycles, the In 3d and the Cd 3d lines can still be clearly identified. However, after 25 dips, those signals have almost disappeared, most likely due to an enhanced signal attenuation of the thicker ILGAR-ZnO top layer. Hence, for ILGAR-ZnO deposited by 25 dips (or more) a complete coverage of the absorber with a layer thickness greater than the information depth of the XPS [around 3 nm (Ref. 16) for 430 eV binding energy using Mg Kα] can be assured. For these samples (25, 50, and 100 dips) only the Zn $L_{23}M_{23}M_{23}$ Auger lines can be observed in Fig. 3. These results support the conclusions drawn from the respective SEM images (Fig. 2).

2. Composition and growth mechanism

The O 1s XPS spectra of the investigated ILGAR-ZnO layers deposited at 90 °C with different numbers of dips are shown in Fig. 4. The broad peaks, some of them with pronounced shoulders, indicate that the ILGAR layers consist of more than one oxygen species. As ILGAR-ZnO layers deposited at low process temperatures still contain a certain amount of hydroxide,[9] both ZnO as well as $Zn(OH)_2$ contributes to the O 1s XPS signal. However, as ILGAR samples are prepared under atmospheric conditions, further contributions to the O 1s emission caused by adsorbed oxygen compounds such as H_2O, O_2, CO, CO_2, or O-containing organic compounds can not be excluded. Oxidic contaminants on the Cd^{2+}/NH_3-treated CIGSSe absorber (see dashed line, 0 dips, in Fig. 4) may also play a role especially for thin ILGAR layers. Other possible contributions might stem from incorporation of H_2O in the ILGAR layers during the dehydration process, due to the rinsing of the sample in H_2O or

Downloaded 31 Aug 2007 to 134.30.24.17. Redistribution subject to AIP license or copyright, see http://jap.aip.org/jap/copyright.jsp

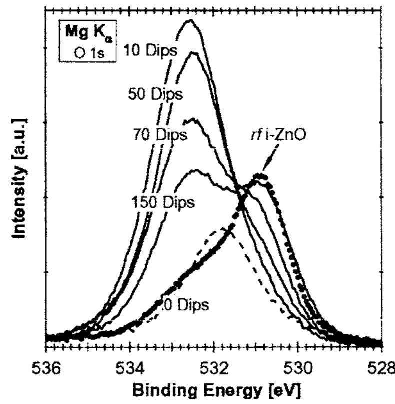

FIG. 4. O 1*s* emission of ILGAR-ZnO layers deposited at 90 °C on Cd^{2+}/NH_3-treated CIGSSe absorbers within 10, 50, 70, and 150 dips (solid lines). For comparison the O 1*s* XPS line is also shown for an rf *i*-ZnO reference (bullets) and for a Cd^{2+}/NH_3 treated, but uncovered CIGSSe substrate ("0 Dip," dashed line).

other O-containing solvents, or from additional deposition process intermediates $[Zn_5(CO_3)_2(OH)_6]$,[15] by-products $[NH_4ClO_4]$ or unconverted precursor salt $[Zn(ClO_4)_2]$.

In order to classify the magnitude of the above mentioned contributions to the O 1*s* photoemission of typical samples investigated in this study an rf-sputtered undoped (intrinsic) *i*-ZnO reference layer (~15 nm) on Cd^{2+}/NH_3-treated CIGSSe was also characterized by XPS for comparison. The corresponding O 1*s* line is presented in the form of bullets in Fig. 4. Although this layer should ideally consist of 100% ZnO, the pronounced shoulder of the O 1*s* XPS line at higher binding energies also points to a contribution of at least one additional oxygen species. Similar reports for rf-sputtered *i*-ZnO can be found in the literature.[20–22] Assuming that the O 1*s* emission is composed of two contributions, the O 1*s* XPS line is fitted by two Voigt functions including a linear background (Fig. 5). As shown by the resulting residual (difference between fit and measured data; lower part of Fig. 5), such an assumption leads to an excellent fit of the experimental data. The determined binding energies (E_{bind}) and full width at half maximum (FWHM) values of the fitted components [I] and [II], respec-

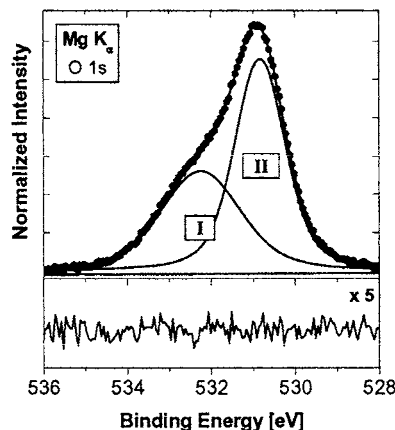

FIG. 5. O 1*s* emission of the rf *i*-ZnO reference (top), experimental data (bullets), and fitted curve (solid lines). The respective residual (difference between fit and experimental data) is also shown (bottom).

TABLE I. Comparison of the determined binding energies for the O 1*s* components [I] and [II] of ILGAR-ZnO layers (dip- and process-temperature variation) as well as of an rf *i*-ZnO sample (regarded as ZnO reference) with data from the literature for the energetic positions of the O 1*s* emission for ZnO and $Zn(OH)_2$.

		Component	E_{bind} (eV)	References
Literature	$Zn(OH)_2$		531.5–532.3	3, 21, and 23–25
	ZnO		530.0–530.9	3 and 20–25
ZnO reference	rf *i*-ZnO	[I]	532.25±0.10	our expt.
		[II]	530.84±0.10	our expt.
Dip variation	ILGAR-ZnO	[I]	532.5±0.20	our expt.
		[II]	530.8±0.10	our expt.
Temperature variation	ILGAR-ZnO	[I]	532.3±0.40	our expt.
		[II]	530.8±0.10	our expt.

tively, are $E_{bind}^{[I]}=(532.25\pm0.10)$ eV, $FWHM^{[I]}=2.25$ eV and $E_{bind}^{[II]}=(530.84\pm0.10)$ eV, $FWHM^{[II]}=1.42$ eV. In the literature, one can find binding energies of the O 1*s* emission for ZnO between 530.0 and 530.9 eV,[2,21–25] which is in good agreement with the main component ([II]) of the O 1*s* XPS line of the rf *i*-ZnO reference. (The essential reference data is compiled in Table I.) Since the considered sample was exposed to ambient air during the transfer into the ultrahigh vacuum (UHV) analysis chamber, H_2O could easily be adsorbed at the rf *i*-ZnO surface, forming a surface $Zn(OH)_2$ layer as proposed in Ref. 26 and thus explaining the observed shoulder at higher binding energies of the O 1*s* XPS line. The comparison of the binding energy of component [I] with literature data for $Zn(OH)_2$ [see Table I, (531.5–532.3) eV (Refs. 2, 21, and 23–25)] supports this conclusion. The larger value for the FWHM of the $Zn(OH)_2$ contribution to the O 1*s* line can be explained by the amorphous nature of this material. Because of the absence of a long-range order it is expected that every single hydroxidic O atom has a different local chemical environment causing slight shifts in the energetic position of the respective emissions and therefore a peak broadening. However, due to the excellent fit and the rather good agreement of measured peak positions with literature values, we subsequently neglect the possible influence of other oxygen compounds than ZnO and $Zn(OH)_2$ in our O 1*s* spectra.

The above considerations concerning the rf *i*-ZnO sample, which is regarded as a ZnO reference, lead to the following model for the quantification of the $ZnO/[ZnO+Zn(OH)_2]$ ratio of the investigated ILGAR layers: It is assumed that the respective O 1*s* emissions are also composed of two contributions ([I]: $Zn(OH)_2$, [II]: ZnO), thus they are also fitted by two Voigt functions. (Note that in contrast to the rf *i*-ZnO sample the hydroxidic component is now not expected to be exclusively situated at the surface, but rather distributed throughout the entire ILGAR layer.) For the fit of the ZnO contribution ([II]) to the O 1*s* emission, the respective FWHM value determined for the rf *i*-ZnO sample was used as reference. Due to an energetic shift in the valence band (not shown) of ILGAR-ZnO layers compared to that of rf *i*-ZnO the corresponding binding energy of component [II] could not be used as reference value. The same holds for the binding energy of component [I] to the O 1*s* XPS line of the

Downloaded 31 Aug 2007 to 134.30.24.17. Redistribution subject to AIP license or copyright, see http://jap.aip.org/jap/copyright.jsp

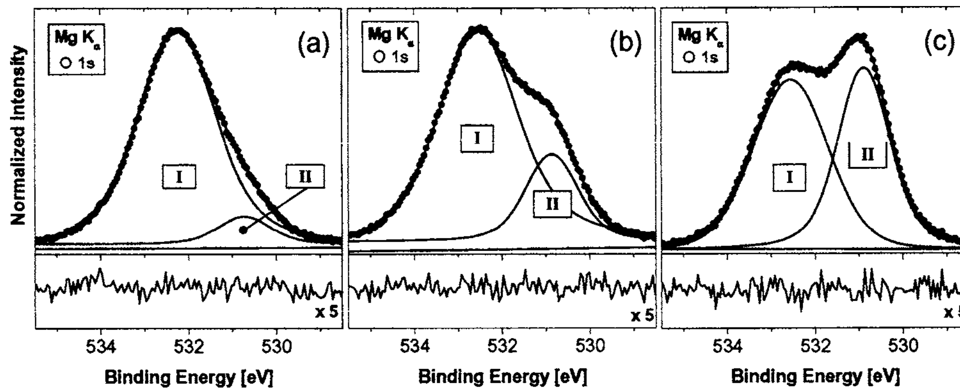

FIG. 6. O 1*s* emission of ILGAR-ZnO layers deposited at 90 °C on Cd^{2+}/NH_3-treated CIGSSe absorbers within 25 (a), 70 (b), and 130 dips (c) (top); experimental data (bullets) and fitted curve (solid lines). The respective residuals (difference between fit and experimental data) are also shown (bottom).

rf *i*-ZnO sample, which is ascribed to $Zn(OH)_2$. In the latter case, also the FWHM value is not useful as reference, because of the amorphous nature of this material. Thus, only the FWHM value of component [II] has been kept constant for all subsequent fits of the O 1*s* XPS lines. Consequently, the FWHM for contribution [I] of the O 1*s* emission, the energetic positions of the components [I] and [II] and their respective intensities and a linear background were refined by the fitting routine.

The application of the above described model to the respective O 1*s* photoemissions of ILGAR-ZnO layers is exemplarily shown in Fig. 6 for the 25, 70, and 130 dip samples. Obviously, also in the case of ILGAR-ZnO, two main oxygen components are sufficient to explain the O 1*s* spectra as indicated by the respective residuals (lower part of Fig. 6). The mean binding energies of contributions [I] and [II] of the O 1*s* emission for all the ILGAR samples of the dip-variation series are (532.5 ± 0.2) eV [FWHM: (2.1 ± 0.1) eV] and (530.8 ± 0.1) eV, respectively. (Note that the specified errors mirror the standard deviation of the respective E_{bind}-values of the contributions [I] and [II] to the O 1*s* line of each single ILGAR sample from the determined mean values.) Since these values are in good agreement with the literature data for $Zn(OH)_2$ and ZnO listed in Table I, and because of the good fits the application of the developed model is justified.

Since the kinetic energy of the photoelectrons of components [I] and [II], respectively, of the O 1*s* emission and hence the corresponding inelastic mean free paths and spectrometer sensitivities are equal, the $ZnO/[ZnO+Zn(OH)_2]$ ratio can directly be calculated from the areas below the corresponding fit curves $[O\ 1s^{[II]}/(O\ 1s^{[II]}+0.5\times O\ 1s^{[I]})]$. The determined surface composition of the ILGAR samples is compared with that of the rf *i*-ZnO reference in Fig. 7. The composition of the ILGAR-ZnO layers does not reach the $ZnO/[ZnO+Zn(OH)_2]$ ratio of the rf *i*-ZnO reference even for a large number of dips, while thin ILGAR-ZnO layers consist mainly of hydroxide. However, one can clearly see that the oxide content of the ILGAR samples increases with increasing number of dips, as we anticipated earlier by analyzing corresponding SEM images (Fig. 2).

The characterization of the bulk composition by Fourier transformed infrared (FTIR) spectroscopy and elastic recoil detection analysis[8,9] (ERDA) has revealed that thick ILGAR samples (200 dips, 90 °C process temperature) contain $\sim$30% $Zn(OH)_2$, which is partially in good agreement with the surface composition of respective thick ILGAR-ZnO layers. However, for rf *i*-ZnO references no hint of any hydroxide (bulk) content was found,[8] which is contrary to their surface composition. This discrepancy points again to the formation of an O–H surface component as proposed above.

Taking the peculiarities of the ILGAR process[6] into account, we propose the following growth model for ILGAR-ZnO layers: During one ILGAR process cycle the sample stays in the heated reaction chamber for 1 min reaching a maximum sample temperature of $\sim$90 °C. This energy input is apparently not sufficient to dehydrate and crystallize the layer of the current process cycle. Further dehydration takes only place during subsequent deposition cycles, resulting in the described formation of bigger ZnO crystallites. It seems that this material conversion is favored in close spatial proximity of already formed ZnO crystallites as indicated by the SEM images [Figs. 2(c)–2(f)]. A high activation energy of the dehydration process was previously concluded from the contradiction between thermodynamic considerations and FTIR analyses.[8] Such a kinetically controlled process may be an explanation for the observed special growth behavior, since the already formed ZnO crystallites could act catalytically, lowering the activation energy and resulting in a favored dehydration of adjacent hydroxidic material.

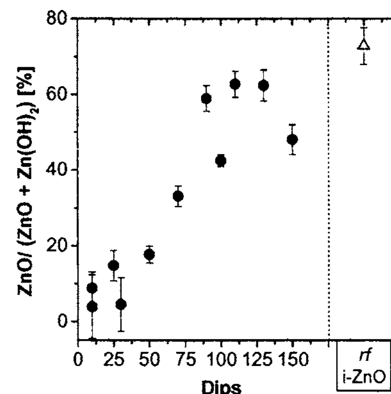

FIG. 7. Surface $ZnO/(ZnO+Zn(OH)_2)$ ratio of ILGAR-ZnO layers deposited at 90 °C on Cd^{2+}/NH_3-treated CIGSSe absorbers prepared within a different number of dips as determined by the accordingly weighted ratio of the areas under the fitted curves visualizing the components [I] and [II] attributed to $Zn(OH)_2$ and ZnO, respectively, of the corresponding O 1*s* XPS lines. For comparison, the corresponding ratio is also depicted for the rf *i*-ZnO reference.

Downloaded 31 Aug 2007 to 134.30.24.17. Redistribution subject to AIP license or copyright, see http://jap.aip.org/jap/copyright.jsp

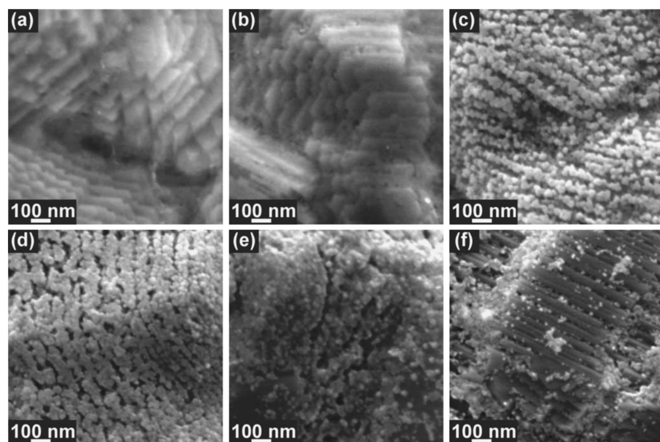

FIG. 8. SEM images of ILGAR-ZnO deposited within 20 dips on Cd^{2+}/NH_3-treated CIGSSe absorbers at process temperatures of 40 (a), 90 (b), 100 (c), 115 (d), 140 (e), and 185 °C (f).

B. Variation of the process temperature

1. Morphology and coverage

ILGAR-ZnO layers were deposited by 20 ILGAR process cycles at process temperatures between 40 and 185 °C on Cd^{2+}/NH_3-treated CIGSSe absorbers. The corresponding SEM images (top view) are shown in Fig. 8. For the ILGAR-ZnO layers prepared at 40 and 90 °C [Figs. 8(a) and 8(b)], a homogeneous layer covering the rough absorber surface, identical to the bottom layer in Fig. 2 can be observed. However, if the process temperature is slightly increased to about 100 °C, a remarkable change in the morphology takes place: Small crystallites embedded in the bottom ILGAR layer appear, especially along the absorber facets. Whereas the ILGAR-ZnO layer deposited at 115 °C seems to be completely composed of crystallites, covering the CIGSSe absorber almost entirely, the coverage of the absorber by ILGAR-ZnO layers prepared above 140 °C is widely lost. For the ILGAR-ZnO layer deposited at 185 °C one can clearly identify the absorber surface, which is only partially covered by individual ZnO crystallites.

Figure 9 shows the corresponding XPS spectra of the In 3*d* and Cd 3*d* photoemissions and the Zn $L_{23}M_{23}M_{23}$ Auger lines of the ILGAR-ZnO/$Cd^{2+}+NH_3$-treated CIGSSe samples prepared at different process temperatures (40, 90, 140, and 185 °C). The exemplary spectra show that at low process temperatures (40 and 90 °C) the signals which are related to the Cd^{2+}/NH_3-treated absorber surface such as In 3*d* and Cd 3*d* are almost completely attenuated. Thus, already 20 dips are obviously sufficient to form an ILGAR-ZnO layer, which almost completely covers the absorber—an observation that further corroborates the visual impression of the corresponding SEM images in Figs. 8(a) and 8(b). However, at process temperatures of 140 and 185 °C, one can clearly identify the In 3*d* XPS signals again. It is noted that in the corresponding survey spectra of these samples (not shown) other absorber-related XPS lines can also be observed. (The signals in the spectrum of the ILGAR sample prepared at 185 °C around 436.5 and 434.9 eV can be attributed to the Mg $K\alpha_{3,4}$ satellites of the in this case especially intense In $3d_{5/2}$ peak.)

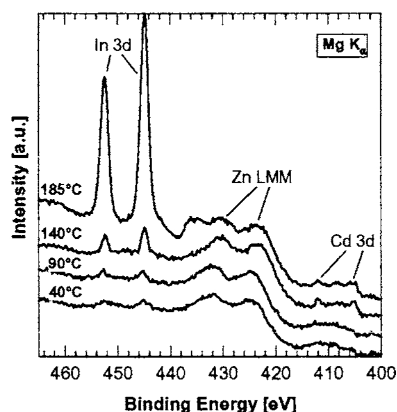

FIG. 9. XPS spectra (region of the In 3*d* and Cd 3*d* XPS lines and the Zn $L_{23}M_{23}M_{23}$ Auger line) of ILGAR-ZnO deposited within 20 dips on Cd^{2+}/NH_3-treated CIGSSe absorbers at process temperatures of 40, 90, 140, and 185 °C.

Both, the appearance of absorber XPS signals and the evidence given by the corresponding SEM images [Figs. 8(e) and 8(f)] implies that at process temperatures above 140 °C the resulting 20 dip ILGAR layers do not cover the rough CIGSSe absorber completely anymore. A possible explanation may be found in a process temperature-dependent ILGAR growth rate, which has been discussed elsewhere.[15] Thus, the ILGAR growth rate depends on the process temperature via the layer composition (see below), as ZnO has a higher density than $Zn(OH)_2$. In addition, the adsorption of the reactant gas at the solid zinc salt precursor during the ILGAR process cycles is reduced at high temperatures[27] strongly decreasing the available amount of reactive species and thus, inhibiting the material conversion. Both effects result in a decreasing growth rate with increasing process temperatures.

In Fig. 9, we find an apparent decrease of the In 3*d*/Cd 3*d* intensity ratio compared to the ratio found for the 10 dip ILGAR-ZnO sample prepared at 90 °C (see Fig. 3). So far no satisfactory explanation can be given for this observation. On one hand, Cd might diffuse into the absorber bulk. On the other hand, the Cd compound, which is deposited on the CIGSSe absorber during the Cd^{2+}/NH_3 treatment,[18] may be removed by the ILGAR process itself at high process temperatures. Future experiments are necessary to clarify this issue.

2. Composition

The O 1*s* emission spectra of the samples prepared at different process temperatures as well as of an rf *i*-ZnO reference are shown in Fig. 10. As in the corresponding spectra of the thickness variation (Fig. 3), the O 1*s* peaks show also features of at least two oxygen species. Furthermore, one can observe that the high binding energy component of the O 1*s* emission is reduced in favor of the contribution to the O 1*s* line at lower binding energies with increasing process temperature (Fig. 10). The spectra in Fig. 10 show clearly that the onset of this intensity redistribution starts above 90 °C and is almost completed already at 100 °C. According to the model developed in Sec. III A this means that the amount of the oxide increases at expense of the hydroxide content in

Downloaded 31 Aug 2007 to 134.30.24.17. Redistribution subject to AIP license or copyright, see http://jap.aip.org/jap/copyright.jsp

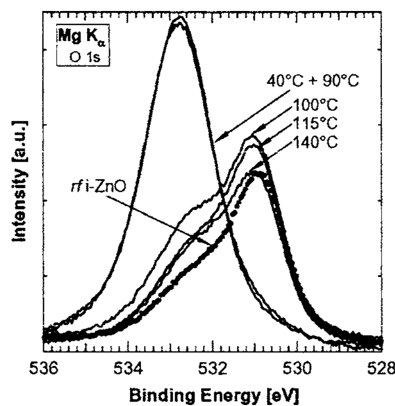

FIG. 10. O 1s emission of ILGAR-ZnO layers deposited within 20 dips on Cd^{2+}/NH_3-treated CIGSSe absorbers at process temperatures of 40, 90, 100, 115, and 140 °C (solid lines). For comparison, the O 1s XPS line is also shown for an rf i-ZnO reference (bullets).

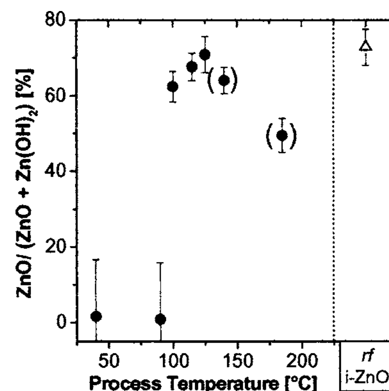

FIG. 12. Surface $ZnO/[ZnO+Zn(OH)_2]$ ratio of ILGAR-ZnO layers deposited within 20 dips on Cd^{2+}/NH_3-treated CIGSSe absorbers prepared at different process temperatures. The ratio was determined by the accordingly weighted ratio of the areas under the fitted curves visualizing the components [I] and [II] attributed to $Zn(OH)_2$ and ZnO, respectively, of the corresponding O 1s XPS lines. For comparison, the corresponding ratio is also depicted for an rf i-ZnO reference. The values for 140 and 185 °C are parenthesized because of the indications of an incomplete coverage of the CIGSSe absorber by the ILGAR layers (see discussion in Sec. III B 1).

the ILGAR-ZnO layer quite suddenly with increasing process temperature. For high process temperatures, the O 1s emission of the ILGAR-ZnO samples even closely resembles the corresponding signal of the rf i-ZnO reference (bullets in Fig. 10), indicating a similar surface composition. Nevertheless, one has to keep in mind that the coverage of the absorber by those ILGAR-ZnO layers is incomplete and that oxygen contributions from the CIGSSe surface might also contribute to the O 1s signal.

The O 1s spectra were subject to the same fitting procedure outlined in Sec. III A. Figure 11 exemplarily shows the result for ILGAR-ZnO layers deposited at 40, 100, and 140 °C process temperature. The corresponding mean binding energies of components [I] and [II] of the entire set of spectra are (532.3 ± 0.4) eV [FWHM: (2.3 ± 0.3) eV] and (530.8 ± 0.1) eV, respectively. The agreement with the corresponding energies found in the literature for ZnO and $Zn(OH)_2$ (Table I) is still satisfactory and in view of the excellent fit obtained in all the spectra (see residuals shown in Fig. 11), we believe that the applied model is still appropriate. However, in comparison to the thickness variation, a higher standard deviation for the binding energy as well as for the FWHM of component [I] is found. Since now the composition of the respective ILGAR layers varies from hydroxide rich to oxide rich (see below) to a higher extent as for the samples of the thickness variation, this can be explained by the extremely different chemical environments for the individual hydroxidic O 1s photoelectrons (see discussion above). Naturally this leads to an increased scattering of the individual binding energies since O 1s contributions from less ordered (amorphous) domains may already be broadened itself.

As described above, the area ratio of the respective O 1s emissions gives the $ZnO/[ZnO+Zn(OH)_2]$ ratio. The resulting surface composition of the ILGAR samples compared with the $ZnO/[ZnO+Zn(OH)_2]$ ratio of the rf i-ZnO reference is shown in Fig. 12. As can be discerned from Fig. 10, the transition from a hydroxide-rich to an oxide-rich surface composition of the ILGAR-ZnO layers is confined to the small temperature range between 90 and 100 °C. For a process temperature of 125 °C, the respective ILGAR layer contains the highest content of oxide (around 70%), which is very close to the rf i-ZnO reference. The complementary characterization of the bulk composition of corresponding (thick) ILGAR layers by ERDA revealed that the oxide content lies between 85% and 90%.[8] The apparent difference between surface and bulk oxide content of 15% and 20% can be explained by the influence of the number of process cycles on the $ZnO/[ZnO+Zn(OH)_2]$ ratio (see Sec. III A) and thus by the kinetics of the ILGAR process. In addition, a formation of an O–H surface component as identified on the

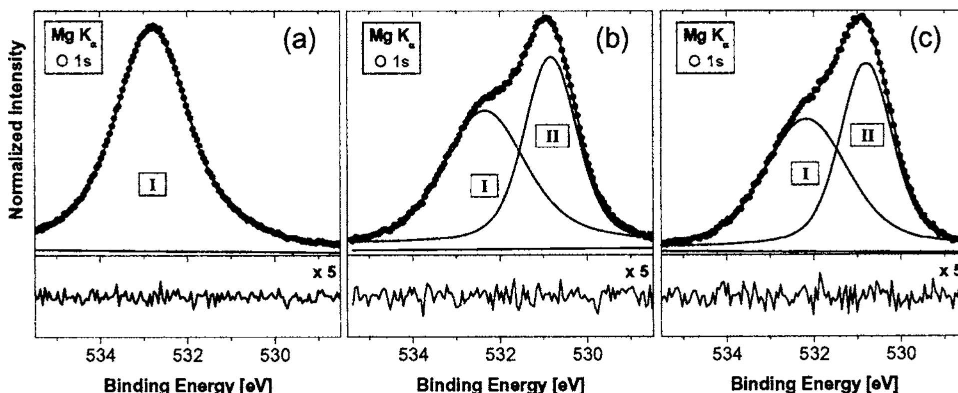

FIG. 11. O 1s emission of ILGAR-ZnO layers deposited within 20 dips on Cd^{2+}/NH_3-treated CIGSSe absorbers at process temperatures of 40 (a), 100 (b), and 140 °C (c) (top); experimental data (bullets) and fitted curve (solid lines). The respective residuals (difference between fit and experimental data) are also shown (bottom).

Downloaded 31 Aug 2007 to 134.30.24.17. Redistribution subject to AIP license or copyright, see http://jap.aip.org/jap/copyright.jsp

rf *i*-ZnO reference might now also be considered for hydroxide-poor ILGAR-ZnO samples prepared at high temperatures.

Finally, we would like to comment on the decreasing $ZnO/[ZnO+Zn(OH)_2]$ ratio for the ILGAR-ZnO layers deposited at 140 and 185 °C in spite of the increasing process temperature (see Fig. 12). Because of the incomplete coverage of the absorber by the ILGAR-ZnO layers in this case (see Sec. III B 1), contributions from the oxidized CIGSSe surface might additionally contribute to the respective O 1*s* spectra. Thus, the determined $ZnO/[ZnO+Zn(OH)_2]$ ratio for these process temperatures might be corrupted. For this reason, the respective ratios in Fig. 12 are kept in parenthesis.

C. Conclusions for CIGSSe-based solar cells with ILGAR-ZnO WEL

The growth mechanism of ILGAR-ZnO on Cd^{2+}/NH_3-treated CIGSSe absorbers discussed in Sec. III A gives a possible explanation for an optimum layer thickness of the ILGAR-ZnO WEL [25–35 dips, see Fig. 1(a)] with which high-efficient solar cells can be obtained. [Note that because of the inconsistent drop of J_{sc}, which can be observed for 35 dips and which was probably caused by an extraneous influence, it is suggested that the optimum number of process cycles is most likely between 25 and 35 dips than around 25 as suggested by the η maximum.] Above this optimum number of process cycles, an increased formation of large, probably well conductive ZnO crystallites is found (Fig. 2), inhibiting a homogeneous coverage of the CIGSSe absorber by the ILGAR-ZnO layer. Consequently, this would reduce the ability of the ILGAR-ZnO WEL to ensure a good (high) shunt resistance (R_{sh}). As a matter of fact, a deterioration primary of the fill factor as well as of the open circuit voltage resulting in a drop of efficiency could be observed for solar cells with ILGAR-ZnO WELs [see Fig. 1(a)] as well as for devices with ILGAR-ZnO "buffers,"[12] if the ILGAR layers are deposited by more than 25–35 dips. For the latter this could indeed be directly correlated with an abrupt drop of R_{sh}.[13]

Taking into account that the process temperature also influences the ability of ILGAR-ZnO layers to cover the rough CIGSSe absorber (see Fig. 8), the drop of FF and V_{oc} and thus of η [see Fig. 1(b)] can also be explained by a low R_{sh} in this context. However, a thermal instability of the CIGSSe absorber, a reaction between WEL and/or reactant gas and the absorber during the ILGAR deposition at high temperatures and/or diffusion processes might also be responsible for the deteriorated device performance as observed for process temperatures above 100 °C.

In addition, the $ZnO/(ZnO+Zn(OH)_2)$ ratio of the surface and surface-near region of ILGAR-ZnO layers changes with both, increasing number of process cycles (Sec. III A 2) and increasing process temperature (Sec. III B 2). In either case, a drop in the device performance of respective solar cells is observed (see Fig. 1). Thus, an alteration of the band alignment at the $WEL/Cd^{2+}+NH_3$-treated CIGSSe heterojunction due to a different composition of the ILGAR-ZnO may also play a role for the deterioration of the PV parameters as reported in Refs. 28 and 29.

IV. SUMMARY AND CONCLUSION

The morphology of $ILGAR\text{-}ZnO/Cd^{2+}+NH_3$-treated CIGSSe samples has been correlated to the surface composition determined by XPS measurements. For process temperatures of up to 90 °C it was found that the oxide content increases steadily with increasing layer thickness. This behavior can explained by the special growth mechanism of the ILGAR layers at this particular process temperature: At first, an amorphous $Zn(OH)_2$ "bottom" layer containing also ZnO nanocrystallites grows, which enables a complete coverage of the rough CIGSSe absorber within 25 process cycles (dips). With increasing layer thickness, the embedded ZnO crystallites increase strongly in size and quantity so that above a certain threshold for the number of process cycles, a homogeneous coverage of the CIGSSe absorber by the ILGAR-ZnO is rather inhibited. Whereas the determined surface composition of thick ILGAR layers are in good agreement with their $ZnO/[ZnO+Zn(OH)_2]$ ratio in the bulk, the difference between surface and bulk composition of thin ZnO samples could be explained by the kinetics of the ILGAR process at 90 °C.

The influence of the process temperature on morphology and composition of ILGAR-ZnO samples at a constant process cycle number of 20 dips revealed that above a process temperature of 90 °C the layer starts to dehydrate and to crystallize. The crystallization process is already completed at 115 °C. If the process temperature is increased beyond 140 °C, respective ILGAR layers do not cover the rough CIGSSe absorber anymore. XPS measurements reveal that the surface composition of the ILGAR-ZnO layers prepared at 115–125 °C is closest to that of our rf-sputtered *i*-ZnO reference.

The observed influence of the ILGAR process parameters (number of process cycles and process temperature) on the layer properties could be correlated with the PV parameters of solar cell devices containing corresponding ILGAR-ZnO layers.

ACKNOWLEDGMENT

The authors are especially thankful to C. Heske, L. Weinhardt, O. Fuchs, E. Umbach (Universität Würzburg), Th. Schedel-Niedrig (Hahn-Meitner-Institut Berlin), and Ch. Jung (BESSY Berlin) for the close collaboration in planning, constructing, and setting up the CISSY end station with them and for numerous helpful discussions. The authors would also like to thank N. Allsop for proofreading the manuscript. Financial support by the German BMBF (Grant No. 01SF0007) and BMWA (Grant No. 0329889) is gratefully acknowledged. Furthermore, one of the authors (M.B.) is grateful to the Deutsche Forschungsgemeinschaft (DFG) for partial financial support within the Emmy-Noether Programm.

Downloaded 31 Aug 2007 to 134.30.24.17. Redistribution subject to AIP license or copyright, see http://jap.aip.org/jap/copyright.jsp

[1]M. A. Contreras, K. Ramanathan, J. AbuShama, F. Hasoon, D. L. Young, B. Egaas, and R. Noufi, Prog. Photovoltaics **13**, 209 (2005).
[2]L. Weinhardt *et al.*, Thin Solid Films **431–432**, 272 (2003).
[3]M. Bär, Ch.-H. Fischer, H.-J. Muffler, S. Zweigart, F. Karg, and M. C. Lux Steiner, Sol. Energy Mater. Sol. Cells **75**, 101 (2003).
[4]J. Möller, Ch.-H. Fischer, H.-J. Muffler, R. Könenkamp, I. Kaiser, C. Kelch, and M. C. Lux-Steiner, Thin Solid Films **361–362**, 113 (2000).
[5]H.-J. Muffler, Ch.-H. Fischer, K. Diesner, and M. C. Lux-Steiner, Sol. Energy Mater. Sol. Cells **67**, 121 (2001).
[6]M. Bär, H.-J. Muffler, Ch.-H. Fischer, and M. C. Lux-Steiner, Sol. Energy Mater. Sol. Cells **67**, 113 (2001).
[7]M. Bär, Ch.-H. Fischer, H.-J. Muffler, B. Leupolt, Th. P. Niesen, F. Karg, and M. C. Lux-Steiner, *Proceedings of the 29th IEEE Photovoltaic Specialists Conference (PVSC)*, New Orleans, 2002, p. 636.
[8]Ch.-H. Fischer, H.-J. Muffler, M. Bär, S. Fiechter, B. Leupolt, and M. C. Lux-Steiner, J. Cryst. Growth **241**, 151 (2002).
[9]E. Strub, M. Bär, W. Bohne, Ch.-H. Fischer, B. Leupolt, S. Lindner, J. Röhrich, and B. Schöneich, Nucl. Instrum. Methods Phys. Res. B **219–220**, 499 (2004).
[10]J. Reichardt *et al.*, Appl. Phys. Lett. **86**, 172102 (2005).
[11]K. Ramanathan *et al.*, *Proceedings of the 26th IEEE Photovoltaic Specialists Conference (PVSC)*, Anaheim, 1997, p. 319.
[12]M. Bär, H.-J. Muffler, Ch.-H. Fischer, S. Zweigart, F. Karg, and M. C. Lux-Steiner, Prog. Photovoltaics **10**, 173 (2002).
[13]M. Bär *et al.*, Prog. Photovoltaics (in press).
[14]J. Palm, V. Probst, W. Stetter, and R. Toelle, Mater. Res. Soc. Symp. Proc. **763**, B6.8.1 (2003), and references therein.
[15]M. Bär, Ph.D. thesis, Technische Universität Berlin, Berlin, 2003; http://edocs.tu-berlin.de/diss/2003/baer_marcus.pdf
[16]D. Briggs and M. P. Seah, *Practical Surface Analysis by Auger and X-ray Photoelectron Spectroscopy* (Wiley, New York, 1983).
[17]M. Bär, U. Bloeck, H.-J. Muffler, M. C. Lux-Steiner, Ch.-H. Fischer, M. Giersig, T. P. Niesen, and F. Karg, J. Appl. Phys. **97**, 014905 (2005).
[18]L. Weinhardt *et al.*, Appl. Phys. Lett. **82**, 571 (2003).
[19]Ch.-H. Fischer, M. Bär, H.-J. Muffler, H. Steigert, Th. Niesen, F. Karg, and M. C. Lux-Steiner, *Proceedings of the Forschungsverbund Sonnenenergie (FVS) TCO-Workshop II*, Jülich, Germany, 16–17 September 2002, p. 69.
[20]F. Säuberlich, J. Fritsche, R. Hunger, and A. Klein, Thin Solid Films **431–432**, 378 (2003).
[21]M. K. Puchert, P. Y. Timbrell, and R. N. Lamb, J. Vac. Sci. Technol. A **14**, 2220 (1996).
[22]L.-J. Meng, C. P. Moreira de Sá, and M. P. dos Santos, Appl. Surf. Sci. **78**, 57 (1994).
[23]L. G. Mar, P. Y. Timbrell, and R. N. Lamb, Appl. Phys. Lett. **60**, 91 (1992).
[24]G. Deroubaix and P. Marcus, Surf. Interface Anal. **141**, 205 (1992).
[25]J. Haber, J. Stoch, and L. Ungier, J. Electron Spectrosc. Relat. Phenom. **9**, 459 (1976).
[26]*Gmelins Handbuch der Anorganischen Chemie—Ergänzungsband Zink*, edited by E. H. E. Pietsch (Verlag Chemie, Weinheim, Germany, 1956), System-Number 32.
[27]K.-H. Näser, *Physikalische Chemie für Technicker und Ingenieure* (VEB Deutscher Verlag für Grundstoffindustrie, Leipzig, 1969).
[28]M. Bär *et al.*, J. Appl. Phys. **98**, 053702 (2005).
[29]Ch.-H. Fischer, M. Bär, Th. Glatzel, I. Lauermann, and M. C. Lux-Steiner, Sol. Energy Mater. Sol. Cells **90**, 1471 (2006).

Downloaded 31 Aug 2007 to 134.30.24.17. Redistribution subject to AIP license or copyright, see http://jap.aip.org/jap/copyright.jsp